Effect of Y on the Oxidation Behavior of a Directionally Solidified Ni-based Single Crystal Superalloy

Zihan Zhao
Science and Technology on Advanced High Temperature Structural Materials Laboratory,Beijing Institute of Aeronautical Materials

Kai Guan
Technology and Science Institute of Northern Taiwan: Taipei City University of Science and Technology

Renjie Cui
Science and Technology on Advanced High Temperature Structural Materials Laboratory,Beijing Institute of Aeronautical Materials

Jianchao Qin
Science and Technology on Advanced High Temperature Structural Materials Laboratory,Beijing Institute of Aeronautical Materials

Zhaohui Huang (huangzhaohui621@163.com)
Science and Technology on Advanced High Temperature Structural Materials Laboratory,Beijing Institute of Aeronautical Materials

Original Article

Keywords: isothermal oxidation, element Y, single crystal superalloy, oxide scale

Posted Date: October 26th, 2020

DOI: https://doi.org/10.21203/rs.3.rs-95133/v1

Effect of Y on the oxidation behavior of a directionally solidified Ni-based single crystal superalloy

Zihan Zhao, Kai Guan, Renjie Cui, Jianchao Qin, Zhaohui Huang*

Science and Technology on Advanced High Temperature Structural Materials Laboratory, Beijing Institute of Aeronautical Materials, Beijing, 100095, China

Abstract

The effect of Y addition on the oxidation behavior of a Ni-based directionally solidified single crystal superalloy was investigated. Isothermal oxidation test for the samples with different-level Y addition was conducted at 1100℃ in air. The Y content of the samples was demarcated by the actual pickup amount resulted from ICP-AES test. It was found that the addition of Y increased the oxide resistance by an adhesive double-layer oxide scale which was composed of Al_2O_3 and spinel $Ni(Cr,Al)_2O_4$. With 70ppm Y addition, the oxidation weight gain was decreased from 12.6g/m^2 for the alloy without Y addition to 5.3g/m^2, and the oxidation rate was significantly decreased. Besides, the internal nitride also disappeared after Y doping because of the increasing oxidation scale adherence and the decreasing of oxidation products. In this study, 660ppm Y addition alloy showed the best oxidation resistance.

Key words: isothermal oxidation; element Y; single crystal superalloy; oxide scale

Introduction

Nickle-based superalloys had been used as the main materials in aerospace industry and industrial gas turbine for years, due to their excellent properties such as high strength, relatively low density and strong environmental resistance at high operating temperature[1-

3]. Turbines, such as high pressure turbine or combustor, are exposed to a high temperature and oxygen-enriched environment, and this means that high mechanical properties have always been required for the using material. And the oxidation resistance at high temperature of alloys mainly achieved by the formation of a passive oxide scale[4].

Rare earth (RE) elements addition can reduce the impurities amount in melt form because of the active properties of RE, and it has brilliant effect on improving the oxidation resistance of alloy by forming an adhesive protective oxide scale which had a low growing rate[5,6]. In 1966, Francis and Whitlow first added yttrium element to Cr-Fe alloy which was proved to improve the oxidation resistance[7]. In the past decades, a number of studies had shown that the addition of RE elements to superalloy was beneficial to improve the oxidation-resistance properties of alloys in high temperature environment[8-10]. But there are still some debates aimed at the mechanism of the influence of RE elements on oxide scale. It was deduced by several references that Y doping could bring better scale adhesion because of the “tying up” effect on S by the RE elements[11-13]. However, all the sulfides formed cases were on the premise that the alloy had high sulfur activity and low oxygen activity. In the caseswith the oppsit premise, sulfides could not be observed in the alloy. From another viewpoint, RE elements would “site block” at the grain boundaries to inhibit the outward diffusion of Al^{3+}[14-16]. Recently, a new perspective was put forward by Arthur H. Heuer and David B. Hovis, that REs could affect oxidation behavior by reducing both the diffusion of O^{2-} to grain boundaries and the Al ionization[17].

Different amount of element Y was added to a directionally solidified nickel-based single crystal superalloy, and the main purpose of the study was to probe into the effect of

Y addition on the oxidation behavior.

Experimental Details

A second-generation nickel-based single crystal superalloy samples with the composition of Ni-7.5Co-7.0Cr-6.2Al-6.5Ta-5.0W-1.5Mo-3.0Re-0.15Hf-0.05C-0.04B(wt%) and different Y doping level were used in this study.

[001] orientation single crystal bars were prepared by the industry Bridgeman directional solidification furnace, in which Y level was changed by using different amount of Ni-Y intermediate alloy. The single crystal bars were subjected to standard heat treatment. According to the ICP-AES results, the final pick-up amount of Y was 70ppm, 190ppm, 230ppm, 660ppm and the corresponding specimens were labeled as 0Y, 70Y, 190Y, 230Y, 660Y, respectively. The specimens for isothermal oxidation experiment were cut into the size of 30mm×10mm×1.5mm from these single crystal bars by electron spark machining, and then they were polished by a series of SiC paper up to 800-grit. The specimens were cleaned by alcohol, followed by blowing dry.

The tested specimens were heated in dry and static air at 1100℃ for 100h, and during the testing they were weighed at an interval of 25h. An X-ray diffractometer was used to characterize the oxide scales at the sample surface. The microstructures of oxide scales and element distribution maps were analyzed by a field emission scanning electron microscope equipped with an energy dispersive spectrometer. The surface roughness was determined by a laser scanning confocal microscope.

During the isothermal oxidation experiment, the weight of porcelain crucible was recorded before the oxidation (m_1) and after every oxidation interval (m_2). The weight gain

per unit of oxidation (G^+) and the average oxidation rate ($\overline{K^+}$) can be calculated according to the following formula:

$$G^+ = \frac{m_2 - m_1}{S}$$

$$\overline{K^+} = \frac{\overline{G^+}}{t}$$

Oxidation Kinetic

Y-doped alloys showed obvious difference from the 0Y sample. Compared to the 0Y sample, Y doping reduced the rate of oxidation and the total weight gain after 100h isothermal oxidation.

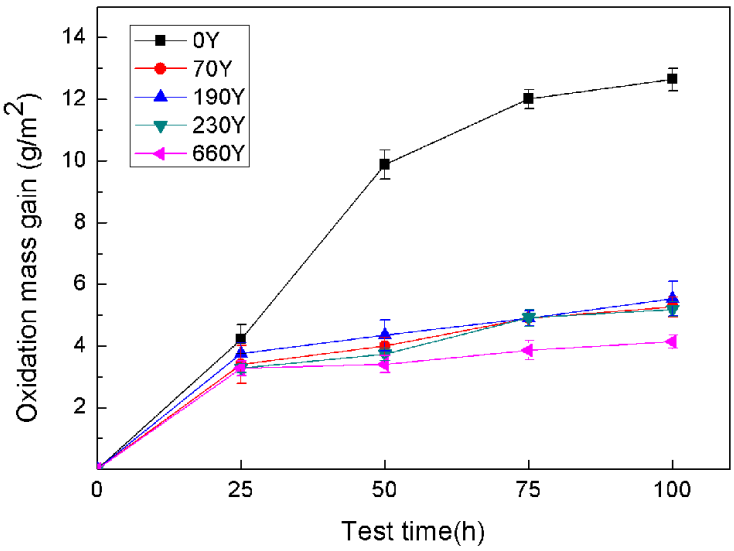

Fig 1 Weight gain of Ni-based single crystal superalloy samples with different Y addition during oxidation test at 1100℃ in air

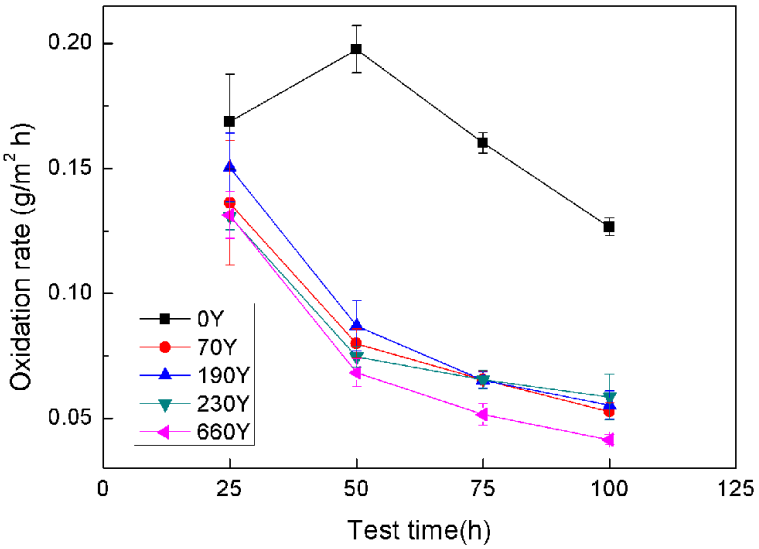

Fig 2 Oxidation rate of Ni-based single crystal superalloy samples with different Y addition during oxidation test at 1100℃ in air

As shown in Fig 1, it was obvious that 0Y sample had the maximum weight gain and the mass gain after oxidation for 100h was 12.6g/m^2. Compared to 0Y sample, the mass gain was decreased for 70Y, 190Y, 230Y, 660Y samples, which was 5.3g/m^2, 5.5 g/m^2, 5.2 g/m^2 and 4.1g/m^2, respectively. Fig 1 also showed clearly that, compared to 0Y, at the earlier stage Y-doped alloy intended to reach a steady state of weight gaining. During the first 25h of oxidation, there was no evident difference of mass gain between each Y-doped specimens. Compared to the Y-doped alloy, 0Y sample still exhibited a high weight gaining after 25h testing. As shown in Fig 3, the oxidation rate of Y-doped alloy continuously decreased, but for 0Y sample, its oxidation rate firstly increased but decreased after 50h testing. During the whole oxidation process, the oxidation rate of 0Y sample was always higher than Y-doped alloys.

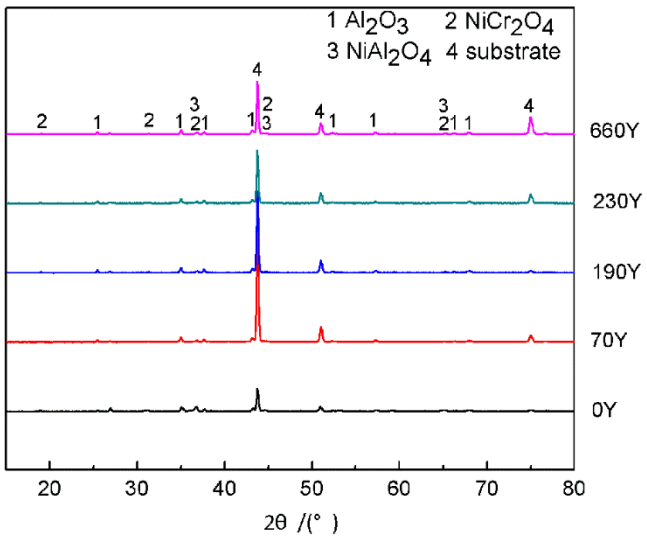

92

93 **Fig 3 XRD pattern of the oxide sale formed on samples with different Y addition after**

94 **oxidation at 1100℃ for 100h**

95 The phase substituents of different samples after oxidation are shown in Fig 2. It

96 appeared that the oxidation products mainly consisted of Al_2O_3 and $Ni(Cr,Al)_2O_4$,.

97 ## Oxidation Scale

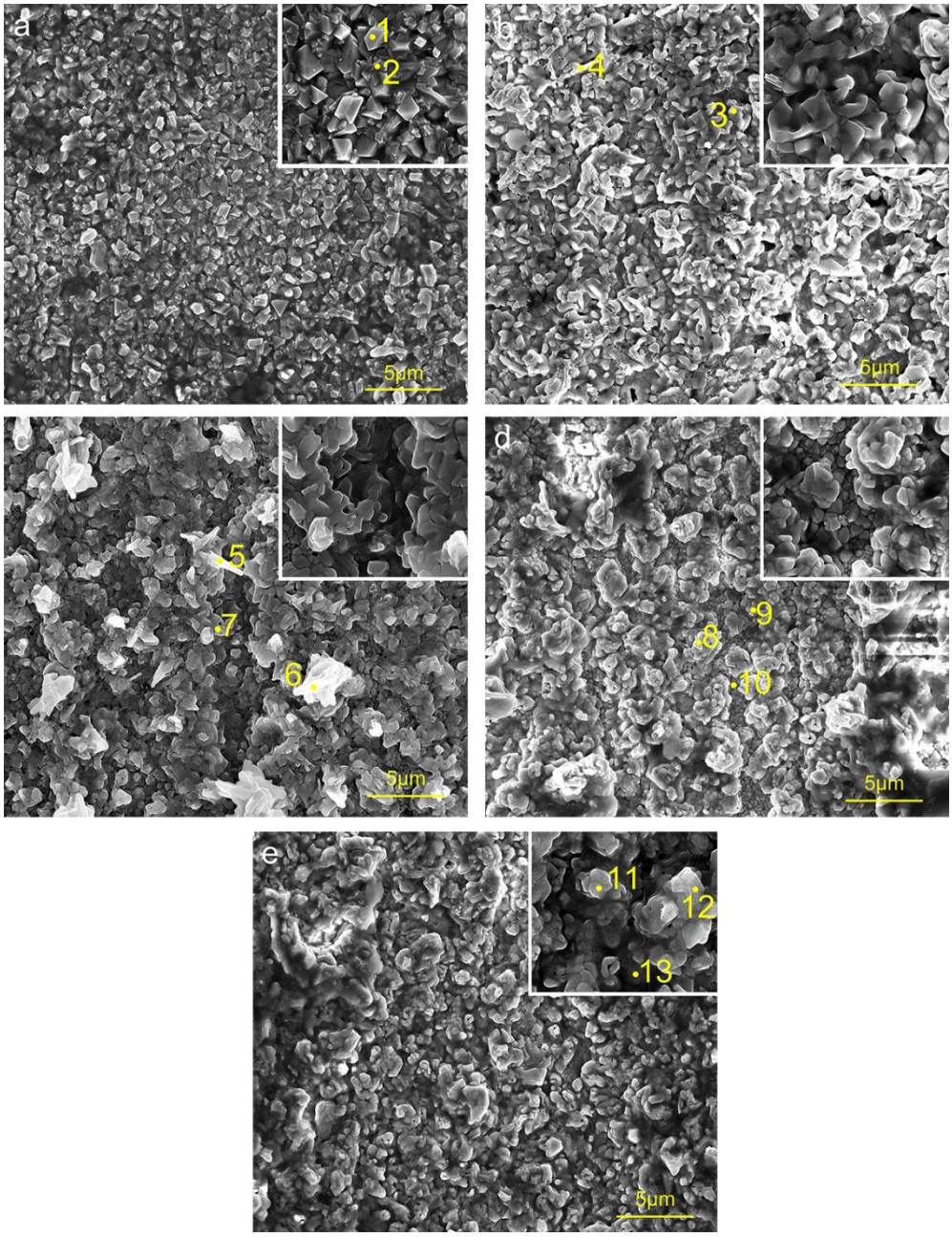

Fig 4 Morphology of the surface oxidation scale of alloy with different Y addition after oxidation at 1100 ℃ (a)0Y; (b)70Y; (c)190Y; (d)230Y; (e)660Y

Table 1 chemical composition of the points marked in Fig 4 (wt. %)

point	C	O	Al	Cr	Co	Ni	Fe
1	19.4	31.5	31.9	4.9	1.9	10.4	-
2	16.6	34.6	30.7	4.8	2.0	11.2	-
3	4.5	25.5	29.3	4.7	-	35.9	-
4	7.9	36.6	26.5	3.8	-	25.2	-
5	9.7	42.5	31.6	3.0	2.4	10.7	0.2
6	12.3	38.1	34.2	3.2	2.3	9.9	-

7	-	48.7	48.2	1.2	0.3	1.7	-
8	17.3	35.7	23.9	4.9	3.1	15.1	-
9	10.2	43.4	42.2	1.6	0.4	2.2	-
10	4.3	11.4	52.2	5.7	3.9	22.4	-
11	-	48.3	46.6	1.5	0.5	2.8	-
12	15.4	38.7	30.6	2.8	2.2	10.4	-
13	9.0	26.0	49.9	3.3	1.7	10.1	-

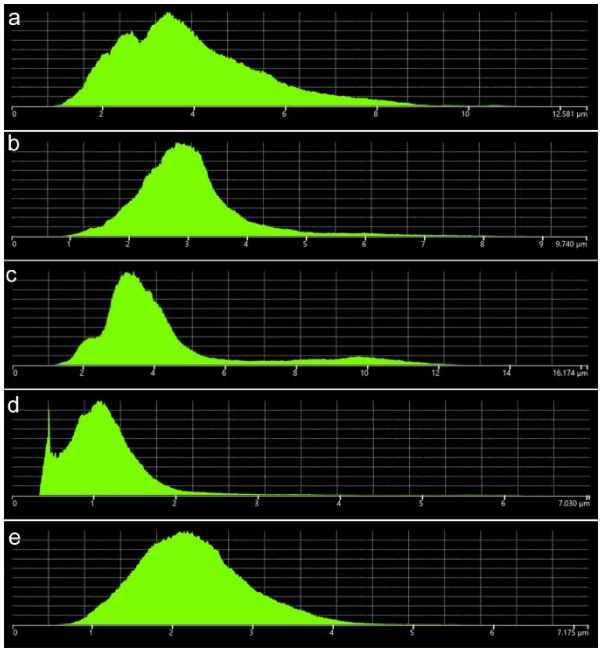

Fig 5 Height histogram resulted by laser scanning confocal microscopy test (a)0Y ; (b)70Y ; (c)190Y ; (d)230Y ; (e)660Y

Fig 4(a-e) showed the surface morphologies of different Y-doped alloy after oxidation at 1100℃ for 100h. There existed lumpy and flaky particles on the oxide scale surface of 0Y sample. The EDS analysis results (Table 1) verified the composition of this kind of sizeable oxide product was $Ni(Cr,Al)_2O_4$.

For 70Y sample, the cubic morphology of oxidation particles on the alloy surface disappeared, the oxidation particles ridged and compactly arranged. With increasing Y amount, the ridged particle began to agglomerate into cauliflower-like bulge. For the agglomerates growing larger continuously, the distance between each agglomerate

114 became closer. Combined with the EDS and XRD results, the main composition of the
115 ridged particulars and agglomerate were both Al_2O_3. Fig 5 was the Height histogram of
116 oxide surface. It could be found that, compared to the 0Y, the roughness decreased in 70Y.
117 And for all Y addition alloys, the roughness of oxide surface tended to first increase and
118 then decrease. The variation of the roughness resulted from the height histogram was in
119 good accordance with the changing tendency of surface morphologies shown in Fig 4.

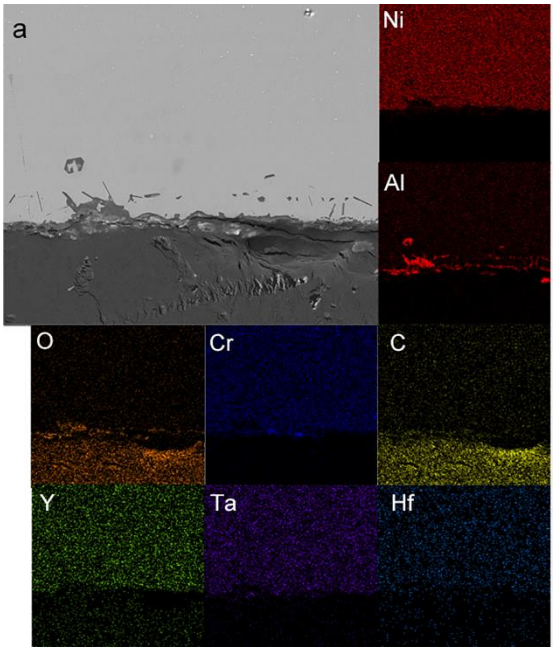

120

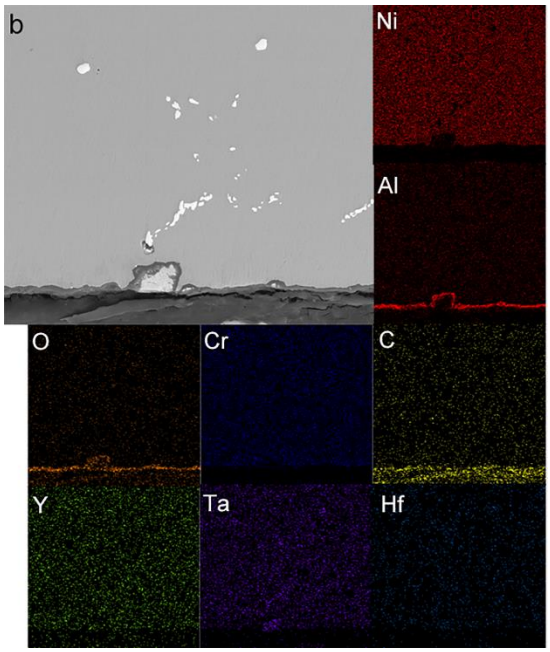

121

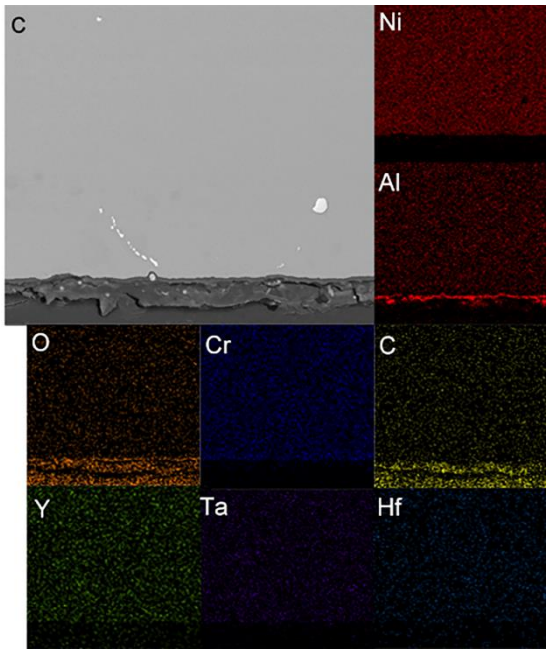

122

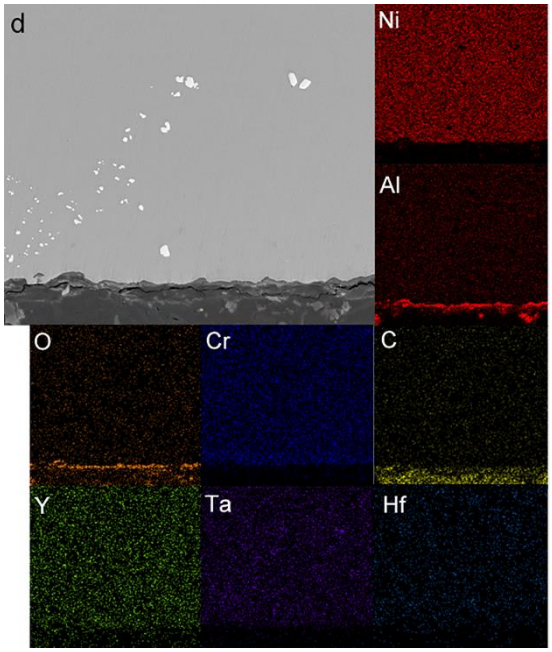

123

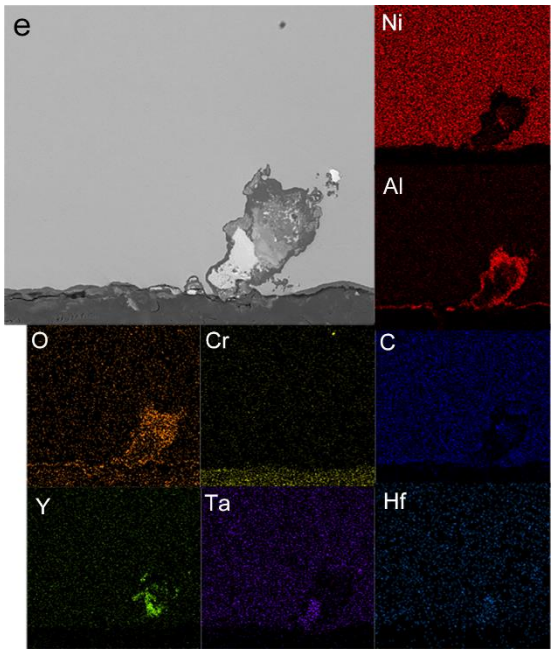

Fig 6 Section morphologies of oxide scale and element area distribution maps of Ni-based superalloy after oxidation at 1100℃ for 100 h

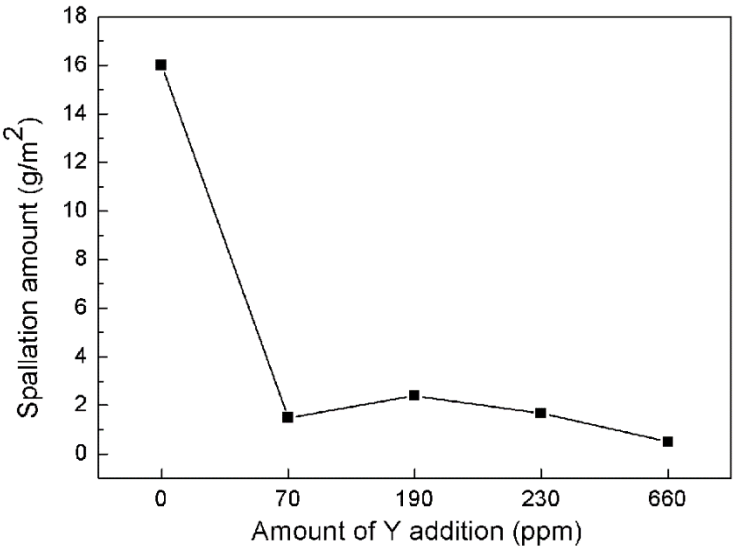

Fig 7 Spallation amount of oxide scale with different Y addition

As shown in Fig 6, all the Y-doped specimens had a continuous Al_2O_3 oxide scale, indicating better oxidation resistance than the alloy without Y addition. This enhancement also reflected in the low dropping weight of oxide scale compared to 0Y(as shown in Fig

7). Needle-like aluminum nitrides determined by EDS existed at the near-surface area in 0Y sample, but they disappeared with the Y addition.

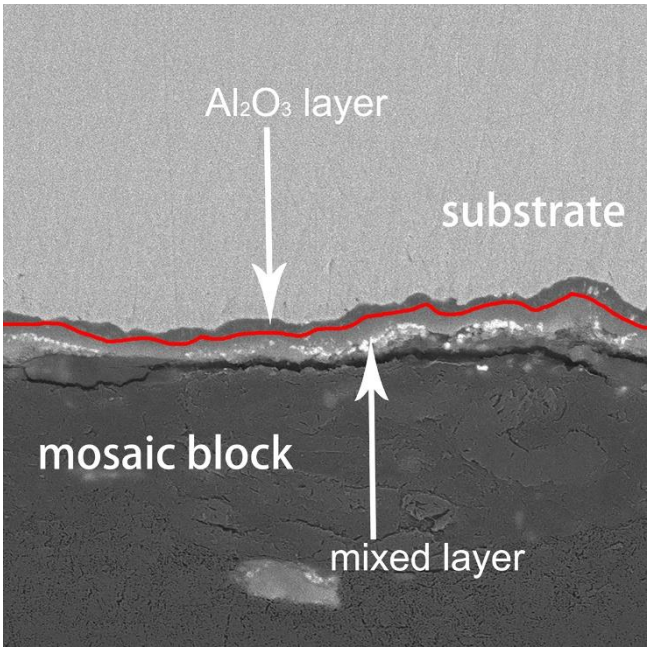

Fig 8 Double-layer structure of oxide scale

Fig 8 showed the classical structure of oxide scale, a typical double-layer structure. Combined with the EDS and XRD analysis results, the outer layer was composed of $Ni(Al,Cr)_2O_4$ spinel and oxide particles containing refractory elements (a mixed oxide layer), and the inner one was Al_2O_3 layer.

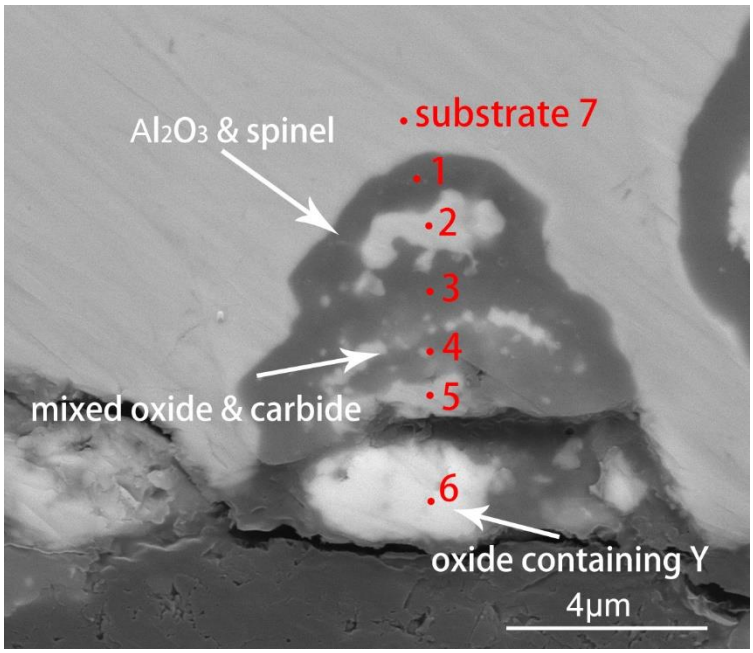

Fig 9 Typical cross-section of surface layer for the Ni-based single crystal superalloy

Table 2 EDS analysis results for the points marked in Fig 9

	Ni	Al	C	O	Cr	Co	Re	Si	N	Hf	S	Y	Ti	Ta
1	29.6	20.5	20.3	14.9	5.0	4.6	2.9	1.6	0.6	0.1	-	-	-	-
2	55.6	5.8	16.9	3.5	1.7	9.6	4.7	2.2	-	-	-	-	0.1	-
3	10.0	26.4	24.0	24.3	4.7	1.7	1.7	1.0	1.0	1.2	-	-	0.1	3.9
4	2.5	21.5	19.8	18.2	15.9	0.3	1.3	1.9	0.9	3.6	-	-	0.1	14.0
5	3.5	8.1	12.3	9.1	19.7	0.8	2.6	2.1	-	7.8	-	-	0.2	33.7
6	8.4	1.9	9.9	14.2	2.0	1.4	3.5	3.1	-	6.6	-	0.5	0.1	48.4
7	55.7	3.0	16.8	0.5	9.1	8.6	4.3	1.9	-	0.2	-	-	0.1	-

While observing the cross-section of oxide scale, within the Y-doped specimens there existed a nail-like internal oxidation, showed in Fig 9. According from the EDS analysis results (Table 2), from inside to outside, the “nail” was composed of Al_2O_3 and spinel, mixture of refractory oxide and carbide, as well as oxide containing Y. It was easy to notice that the Y contained oxide located at the bottom of “nail”.

Table 3 Characteristics of the oxide scale for different levels of Y addition

	70Y	190Y	230Y	660Y
Thickness of oxide scale(μm)	2.799	1.987	2.435	1.882
Spallation amount (g/m^2)	1.500	2.400	1.683	0.500
Oxidation weight gain(g/m^2)	5.264	5.525	5.180	4.135

Table 3 showed the change of oxide scale thickness, spallation amount of oxide scale and the oxidation weight gain with the added amount of element Y. Therefore, from these three aspects it could be concluded that 660Y alloy sample exhibited the best oxidation resistance among all of the Y-doped samples.

Discussion

The initial oxidized products was NiO and spinel ($Ni(Cr,Al)_2O_4$), in which NiO firstly formed with the oxidation process but it finally disappeared as the intermediate product because it reacted with Al_2O_3 and Cr_2O_3 forming $Ni(Cr,Al)_2O_4$[18]. This can be described by the following expression:

$$NiO+Cr_2O_3/Al_2O_3 \rightarrow Ni(Al,Cr)_2O_4$$

With the addition of Y element, the phenomenon of oxide scale spallation almost disappeared, and thus the oxidation resistance of the alloy was increased significantly.

According to the classic Wagner theory, the oxidation process was orientational and determined by the direction of ions diffusion[19,20]. According to the study on NiCrAls and FeCrAls, the oxide scales formation involved both outward aluminum diffusion and inward oxygen diffusion, and the pathway of the oxidizing process was along those grain boundaries[21-23].

For the analysis result of oxidation kinetic curves, the oxidation resistance increased with the addition of Y element, and 660ppm Y addition alloy exhibited the best oxidation resistance.

And for the high chemical activity of element Y, segregation of Y ions would occur at the matrix/oxide scales interface[24]. Because of the lager standard Gibbs formation free

energy (ΔG^{θ}) of Y_2O_3, the affinity of Y with O was stronger than that of C with Al[25,26], and thus Y_2O_3 formed at surface prior to the Al_2O_3 layer. The formation of Y_2O_3 appears to affect the Al^{3+}/O^{2-} diffusion behavior at the grain boundaries[19,27,28], but no evidence for significant segregation of Al^{3+} and O^{2-} was found.

For 0Y sample, needle-like aluminum nitrides existed at the near-surface region of oxidation scale in the matrix. Due to the volume increasing, which was caused by the formation of the oxides (Al_2O_3 28% increasing)[29,30], cracks and spallation occurred there. Cracks were indeed observed across the oxide scales and element N further penetrated through the cracks to form AlN. However, with Y doping, the aluminum nitrides disappeared because of the higher oxide scale adherence and less oxidation products, as well as less volume increasing below oxide scale and in the meantime the cracks also disappeared. On the other hand, according to the references[31,32], this kind of phenomenon is also related to the purification of alloy after the addition of Y element.

Conclusion

Based on the study of the oxidation kinetic and the surface/cross-section morphologies of oxidation scale, some key points can be summarized as follows:

1. For improving the oxidation resistance of Ni-based superalloy, doping yttrium was significantly effective by decreasing the oxidation rate, and after oxidation at 1100℃ for 100h the weight gain of the 70 ppm Y alloy decreased from 12.6g/m^2 to 5.3g/m^2. Furthermore, the 660Y alloy exhibited the best oxidation resistance due to the least weight gain, spallation amount and thickness of oxide scale.

2. The alloy chosen in this study was Al_2O_3 formation alloy, and it has a typical double-layer structure of the oxide scale, one with the main composition of Al_2O_3 and $Ni(Al,Cr)_2O_4$ spinel, and the other with oxide/carbide particles containing refractory elements.

3. With Y addition, the needle-like aluminum nitrides disappeared resulted from the formation of adhesive oxide scale and the decreasing of oxide products which led to less increasing of oxide volume, and in the meantime the cracks also disappeared in oxide scale.

Declarations

Availability of data and materials

The datasets used and/or analysed during the current study are available from the corresponding author on reasonable request.

Competing interests

The authors declare that they have no competing interests.

Funding

The work was supported by the preliminary research project.

Authors' contributions

ZHZ and KG were in charge of the whole trial; ZHZ wrote the manuscript; RJC and JCQ assisted with sampling and laboratory analyses; ZHH assisted with the revision. All authors read and approved the final manuscript.

Acknowledgements

Not applicable.

References:

[1]Sato, A., Chiu, Y. L., & Reed, R. C. (2011). Oxidation of nickel-based single-crystal superalloys for industrial gas turbine applications. *Acta Materialia, 59*(1), 225-240.

[2]Darolia, R. (2018). Development of strong, oxidation and corrosion resistant nickel-based superalloys: critical review of challenges, progress and prospects. *International Materials Reviews, 64*, 1-26. doi:10.1080/09506608.2018.1516713

[3]Caron, P., & Lavigne, O. (2011). Recent studies at Onera on superalloys for single crystal turbine blades. (3), p. 1-14. Retrieved from https://hal.archives-ouvertes.fr/hal-01183625.

[4]Zhang, Y., Luo, H., Zhong, Q., Yu, H., & Lv, J. (2019). Characterization of Passive Films Formed on As-received and Sensitized AISI 304 Stainless Steel. *Chinese Journal of Mechanical Engineering, 32*(1), 27. Retrieved from https://doi.org/10.1186/s10033-019-0336-8. doi:10.1186/s10033-019-0336-8

[5]Guo, T. B., Zhang, F., Ding, W. W., & Jia, Z. (2018). Effect of micro-scale Y addition on the fracture properties of Al–Cu–Mn alloy. *Chinese Journal of Mechanical Engineering, 31*(06), 217-227.

[6]Jin, H., & Felix, A. (2008). Influence of rare earth doping on mechanical property and micro-structure of chromia oxide film. *Chinese Journal of Mechanical Engineering*(03), 16-19.

[7]Francis, J. M., & Whitlow, W. H. (1966). The morphology of oxide film growth on AISI type 304 stainless steel in high temperature water at 300° and 350° C. *Journal of Nuclear Materials, 20*(1), 1-10.

[8]Stringer, J. (1989). The reactive element effect in high-temperature corrosion. *Materials Science and Engineering: A, 120-121*, 129-137. Retrieved from http://www.sciencedirect.com/science/article/pii/0921509389907302. doi:https://doi.org/10.1016/0921-5093(89)90730-2

[9]Moon, D. P. (1989). The reactive element effect on the growth rate of nickel oxide scales at high temperature. *Oxidation of Metals, 32*(1-2), 47-66.

[10]Tawancy, H. M. (1991). On the role of yttrium during high-temperature oxidation of an Ni-Cr-Al-Fe-Y alloy. *Metallurgical Transactions A, 22*(6), 1463-1465. Retrieved from https://doi.org/10.1007/BF02660678. doi:10.1007/BF02660678

[11]Smialek, J. L., Jayne, D. T., Schaeffer, J. C., & Murphy, W. H. (1994). Effects of hydrogen annealing, sulfur segregation and diffusion on the cyclic oxidation resistance of superalloys: a review. *Thin Solid Films, 253*(1–2), 285-292.

[12]Smialek, J. L., & Pint, B. A. (2001). Optimizing scale adhesion on single crystal superalloys. *Materials Science Forum, 369–372*, 459-466. doi:https://doi.org/10.4028/www.scientific.net/msf.369-372.459

[13]Aimone, P. R., & McCormick, R. L. (1992). The Effects of Yttrium and Sulfur on the Oxidation Resistance of an Advanced Single Crystal Nickel Based Superalloy. In *Superalloys 1992* (pp. 817-823).

[14]Pint, B. A. (1996). Experimental observations in support of the dynamic-segregation theory to explain the reactive-element effect. *Oxidation of Metals, 45*(1/2), 1-37.

[15]Yun, D. W., Seo, S. M., Jeong, H. W., & Yoo, Y. S. (2020). The effect of Gd addition on the cyclic oxidation behavior and creep life of alumina-forming Ni-based superalloy. *Corrosion Science, 170*, 108694. Retrieved from

http://www.sciencedirect.com/science/article/pii/S0010938X19316385. doi:https://doi.org/10.1016/j.corsci.2020.108694

[16]Swadźba, R., Swadźba, L., Wiedermann, J., Hetma ń czyk, M., & Witala, B. (2014). Characterization of alumina scales grown on a 2nd generation single crystal Ni superalloyduring isothermal qxidation at 1050, 1100 and 1150 °C. *Oxidation of Metals, 82*(3), 195-208. Retrieved from https://doi.org/10.1007/s11085-014-9487-2. doi:10.1007/s11085-014-9487-2

[17]Heuer, A., Hovis, D., Smialek, J., & Gleeson, B. (2011). Alumina scale formation: a new perspective. *Journal of the American Ceramic Society, 94*, s146-s153. doi:10.1111/j.1551-2916.2011.04573.x

[18]Hussain, N., Shahid, K. A., & Rahman, I. H. K. (1995). Oxidation of high-temperature alloys (superalloys) at elevated temperatures in air. II. *Oxidation of Metals*.

[19]Heuer, A. H., Nakagawa, T., Azar, M. Z., Hovis, D. B., Smialek, J. L., Gleeson, B., . . . Tangney, P. (2013). On the growth of Al_2O_3 scales. *Acta Materialia, 61*(18), 6670-6683.

[20]Wagner, & Carl. (1933). Beitrag zur Theorie des Anlaufvorgangs. *Ztschrift Für Physikalische Chemie, 21B*(1), 25-41.

[21]Quadakkers, W. J., Elschner, A., Speier, W., & Nickel, H. (1991). Composition and growth mechanisms of alumina scales on FeCrAl-based alloys determined by SNMS. *Applied Surface ence, 52*(4), 271-287.

[22]Guo, H., Di, W., Hui, P., Gong, S., & Xu, H. (2014). Effect of Sm, Gd, Yb, Sc and Nd as reactive elements on oxidation behaviour of β-NiAl at 1200 °C. *Corrosion Science, 78*(jan.), 369-377.

[23]Prescott, R., Mitchell, D. F., Graham, M. J., & Doychak, J. (1995). Oxidation mechanisms of β-NiAl + Zr determined by SIMS. *Corrosion Science, 37*(9), 1341-1364.

[24]Yang, Y., Zhang, T., Shao, Y., Meng, G., & Wang, F. (2013). New understanding of the effect of hydrostatic pressure on the corrosion of Ni–Cr–Mo–V high strength steel. *Corrosion Science, 73*(aug.), 250-261.

[25]Bian, W., Zhang, H., Zhang, X., Gao, M., Li, J., Li, Q., . . . Zhang, H. (2019). Comprehensive influence of Y on K417 superalloy: Purification, interactions among the alloy elements and high temperature properties. *Materials Science and Engineering A, 755*(MAY 7), 190-200.

[26]Li, Q. L., Zhang, H. R., Gao, M., Li, J. P., Tao, T. X., & Zhang, H. (2018). Mechanisms of reactive element Y on the purification of K4169 superalloy during vacuum induction melting. *矿物冶金与材料学报(英文版), 25*(6), 696-703.

[27]Birks, N., Meier, G. H., & Pettit, F. S. (2006). *Introduction to the High Temperature Oxidation of Metals* (2 ed.). Cambridge: Cambridge University Press.

[28]Guohua, Y. F. Y., Sinica, A., Shanghai, Hefei, & Shenvang. (1992). Effect of reactive elements Y and Ce on high temperature oxidation of Fe-25Cr-40Ni alloy. *Acta Metallurgica Sinica*(11), 383-390.

[29]Pfennig, A., & Fedelich, B. (2008). Oxidation of single crystal PWA 1483 at 950 °C in flowing air. *Corrosion Science, 50*(9), 2484-2492.

[30]Litz, J., Rahmel, A., & Schorr, M. (1988). Selective carbide oxidation and internal nitridation of the Ni-base superalloys IN 738 LC and IN 939 in air. *Oxidation of Metals, 30*(1-2), 95-105.

[31]Guimarães, A. V., Silveira, R. M. S. D., Almeida, L. H. D., Araujo, L. S., & Dille, J. A. F. (2020). Influence of yttrium addition on the microstructural evolution and mechanical properties

of superalloy 718. *Materials Science and Engineering A, 776*, 139023.

[32]Bian, W. D., Zhang, H. R., Gao, M., Li, Q. L., Li, J. P., Tao, T. X., & Zhang, H. (2018). Influence of yttrium and vacuum degree on the purification of K417 superalloy. *Vacuum*, S0042207X18300976.

Figures

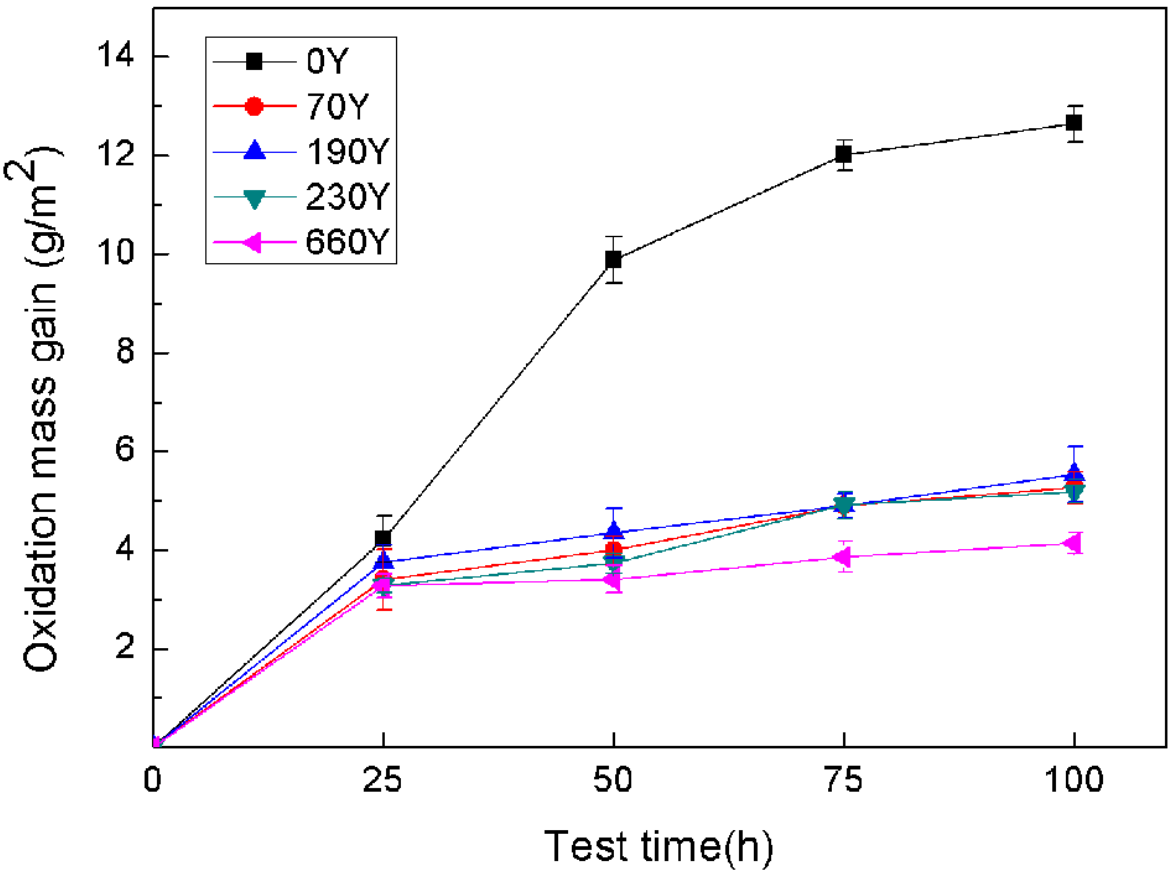

Figure 1

Weight gain of Ni-based single crystal superalloy samples with different Y addition during oxidation test at 1100℃ in air

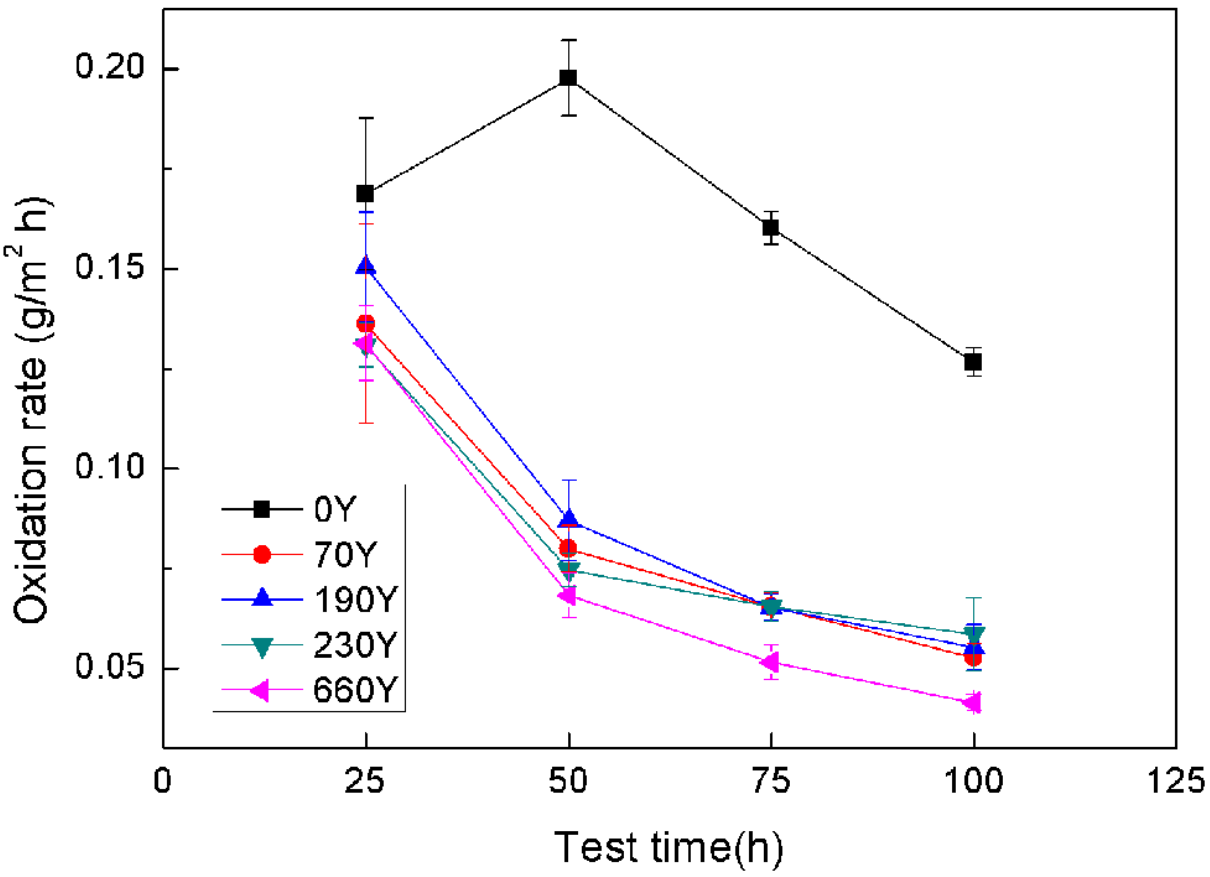

Figure 2

Oxidation rate of Ni-based single crystal superalloy samples with different Y addition during oxidation test at 1100℃ in air

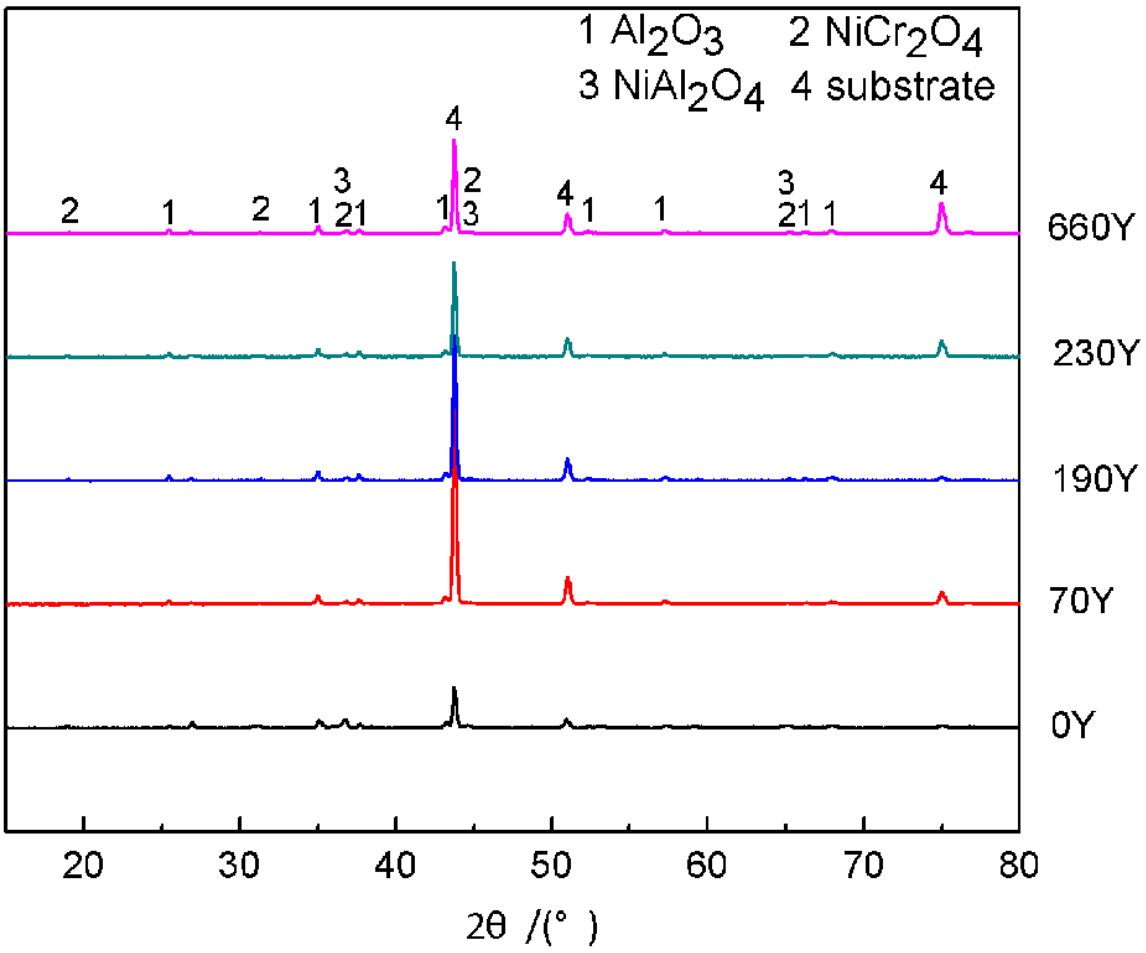

Figure 3

XRD pattern of the oxide sale formed on samples with different Y addition after oxidation at 1100℃ for 100h

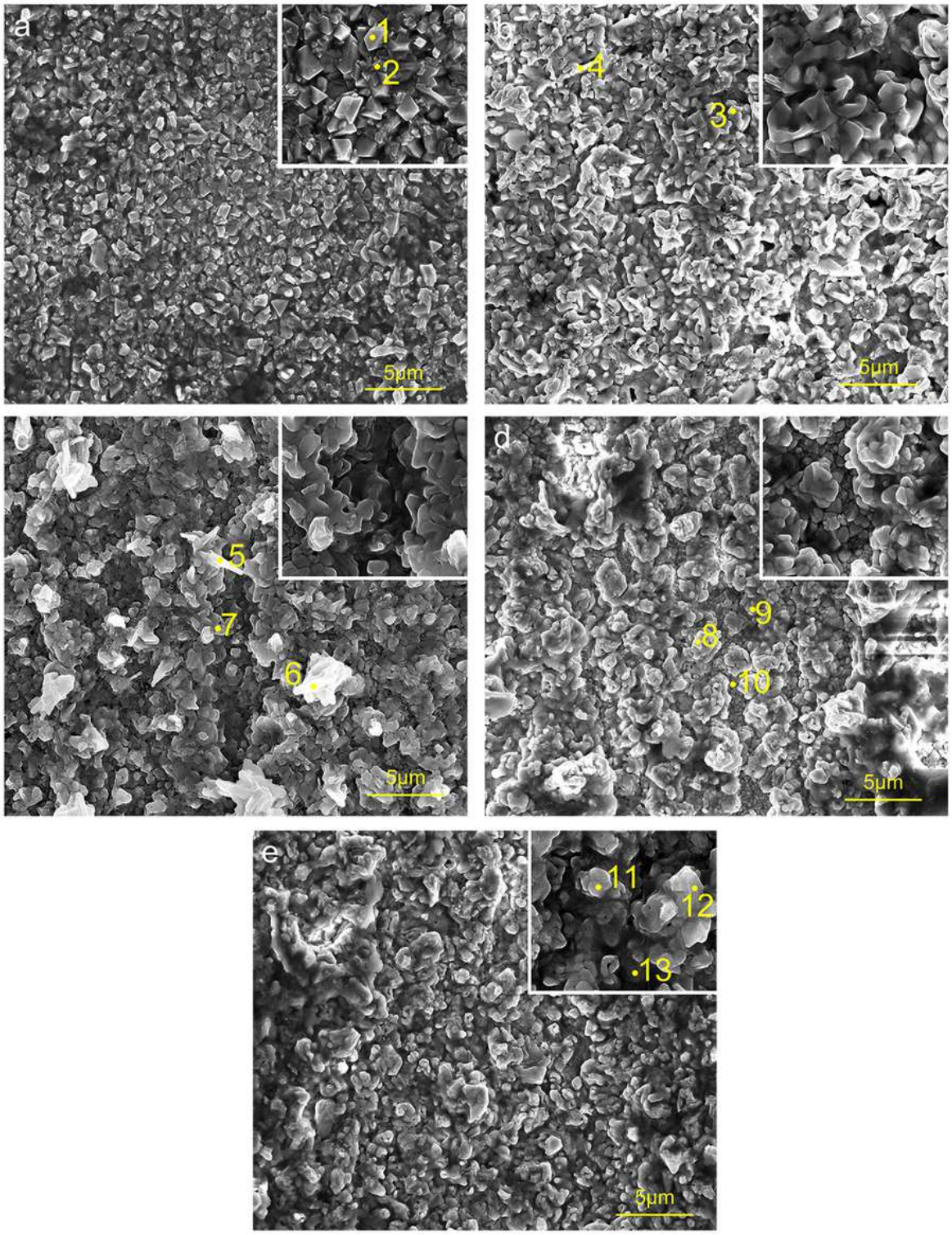

Figure 4

Morphology of the surface oxidation scale of alloy with different Y addition after oxidation at 1100 □ (a)0Y; (b)70Y; (c)190Y; (d)230Y; (e)660Y

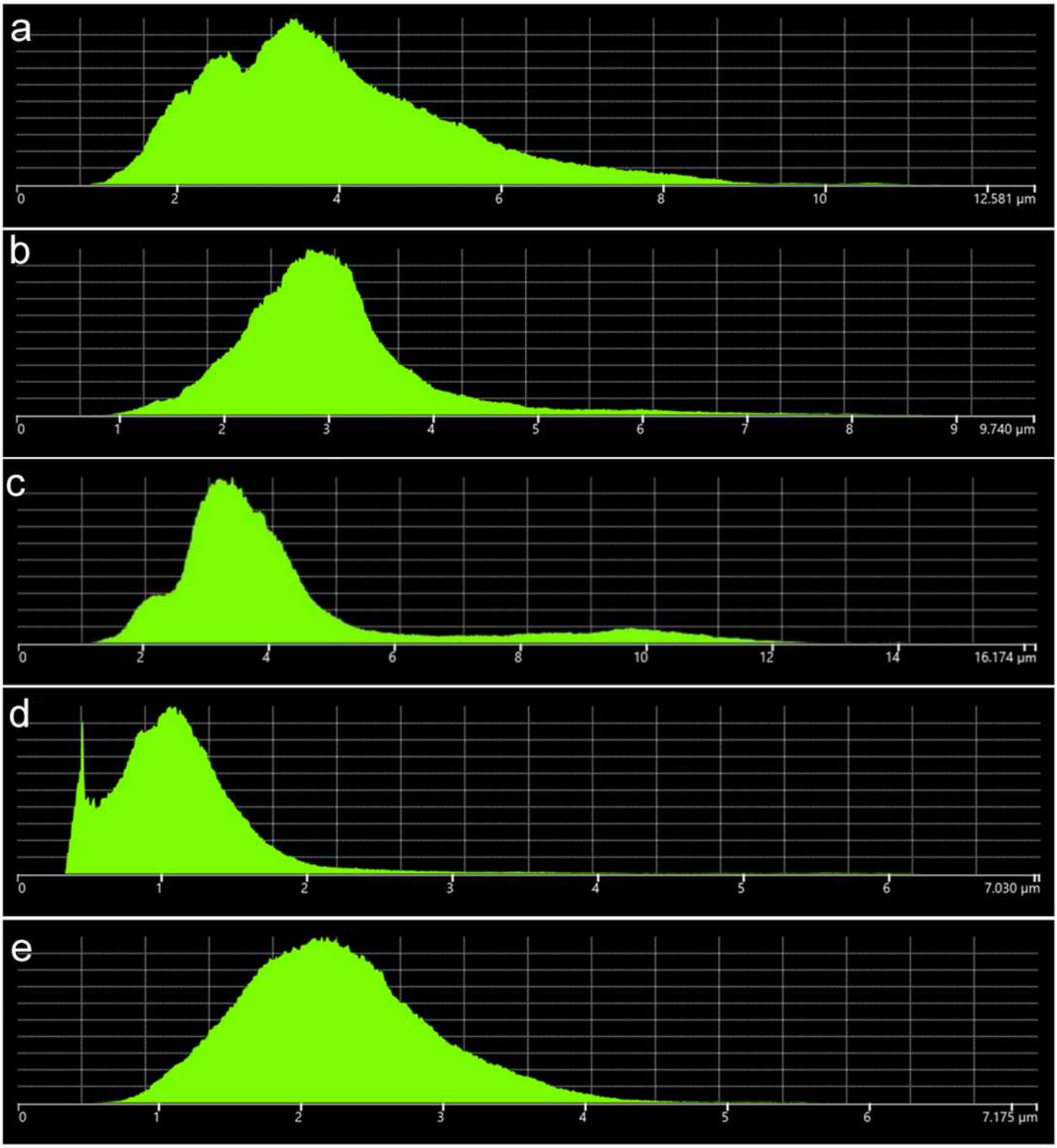

Figure 5

Height histogram resulted by laser scanning confocal microscopy test (a)0Y ; (b)70Y ; (c)190Y ; (d)230Y ; (e)660Y

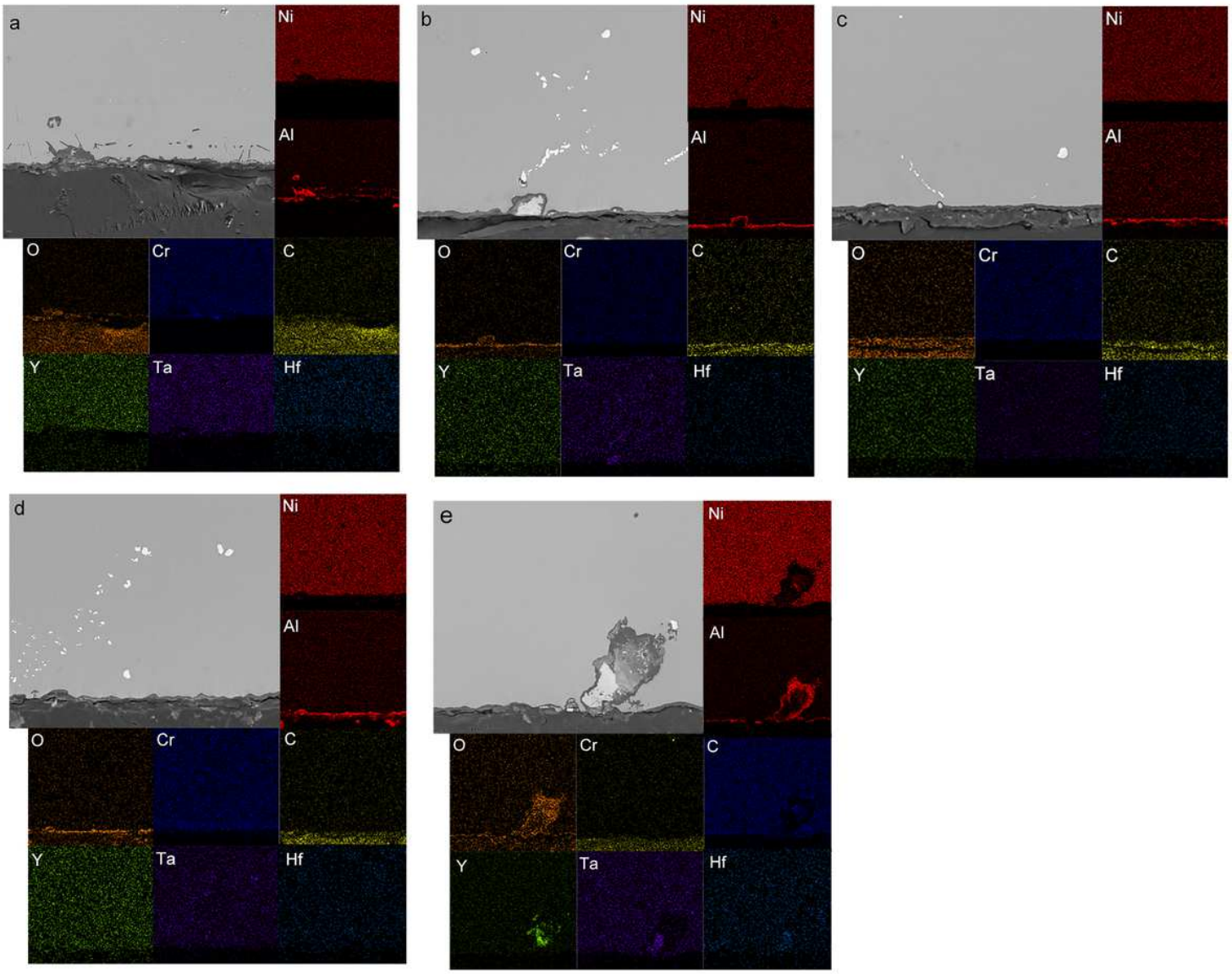

Figure 6

Section morphologies of oxide scale and element area distribution maps of Ni- based superalloy after oxidation at 1100℃ for 100 h

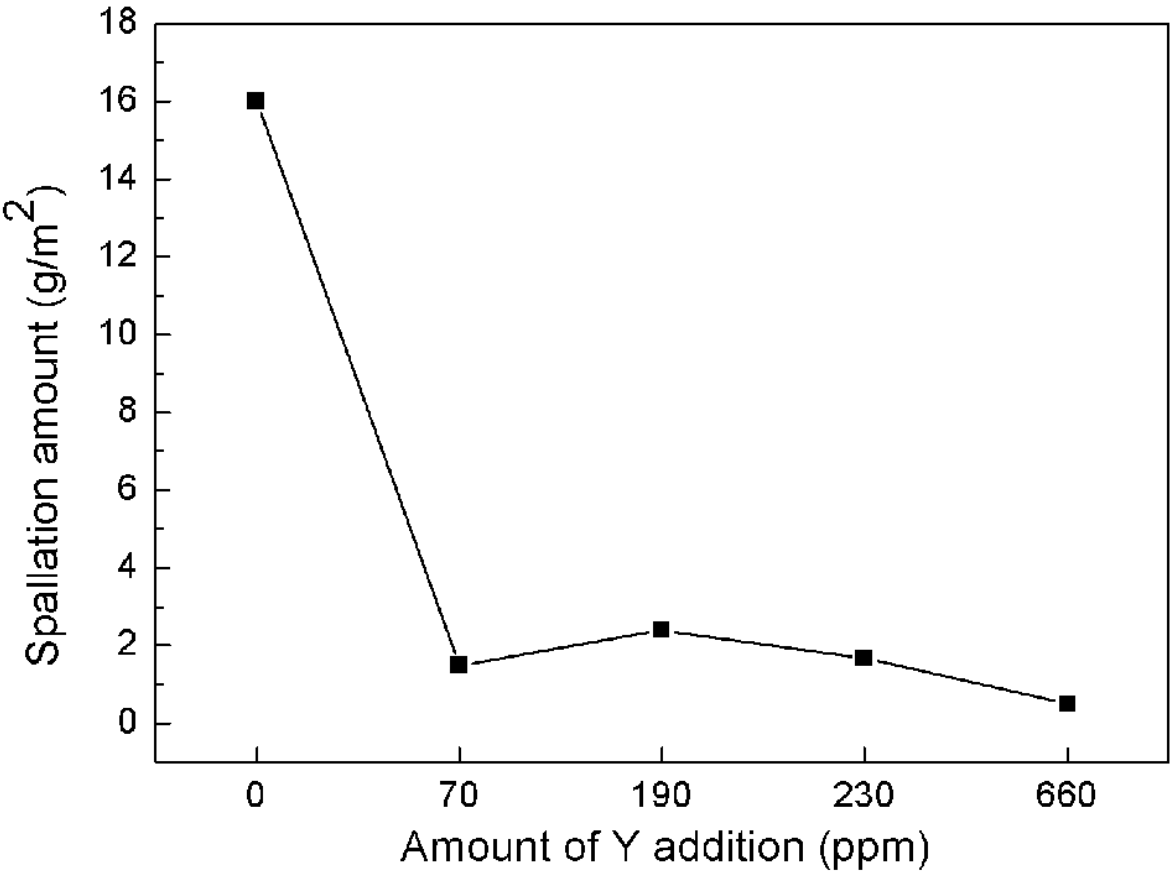

Figure 7

Spallation amount of oxide scale with different Y addition

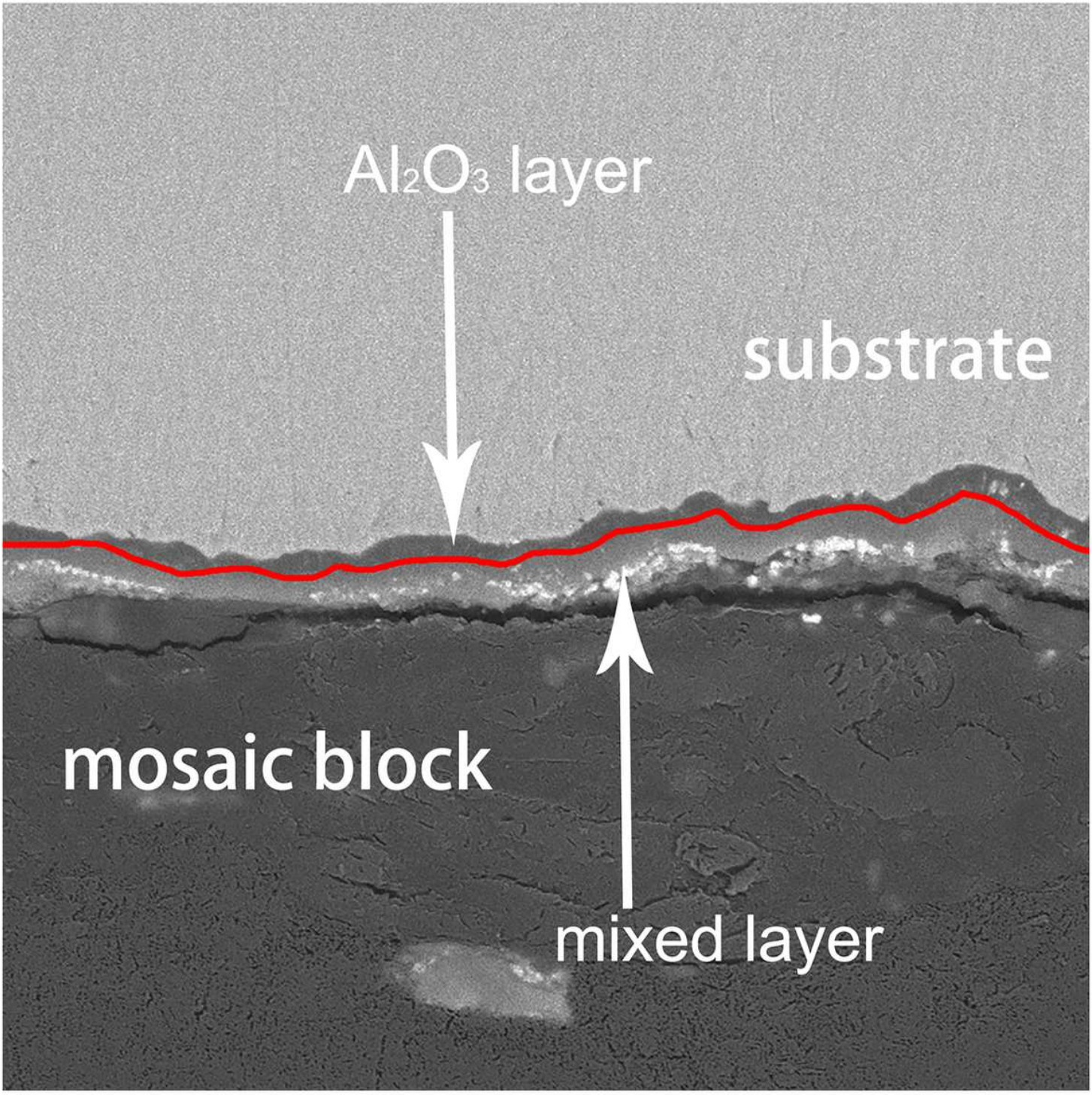

Figure 8

Double-layer structure of oxide scale

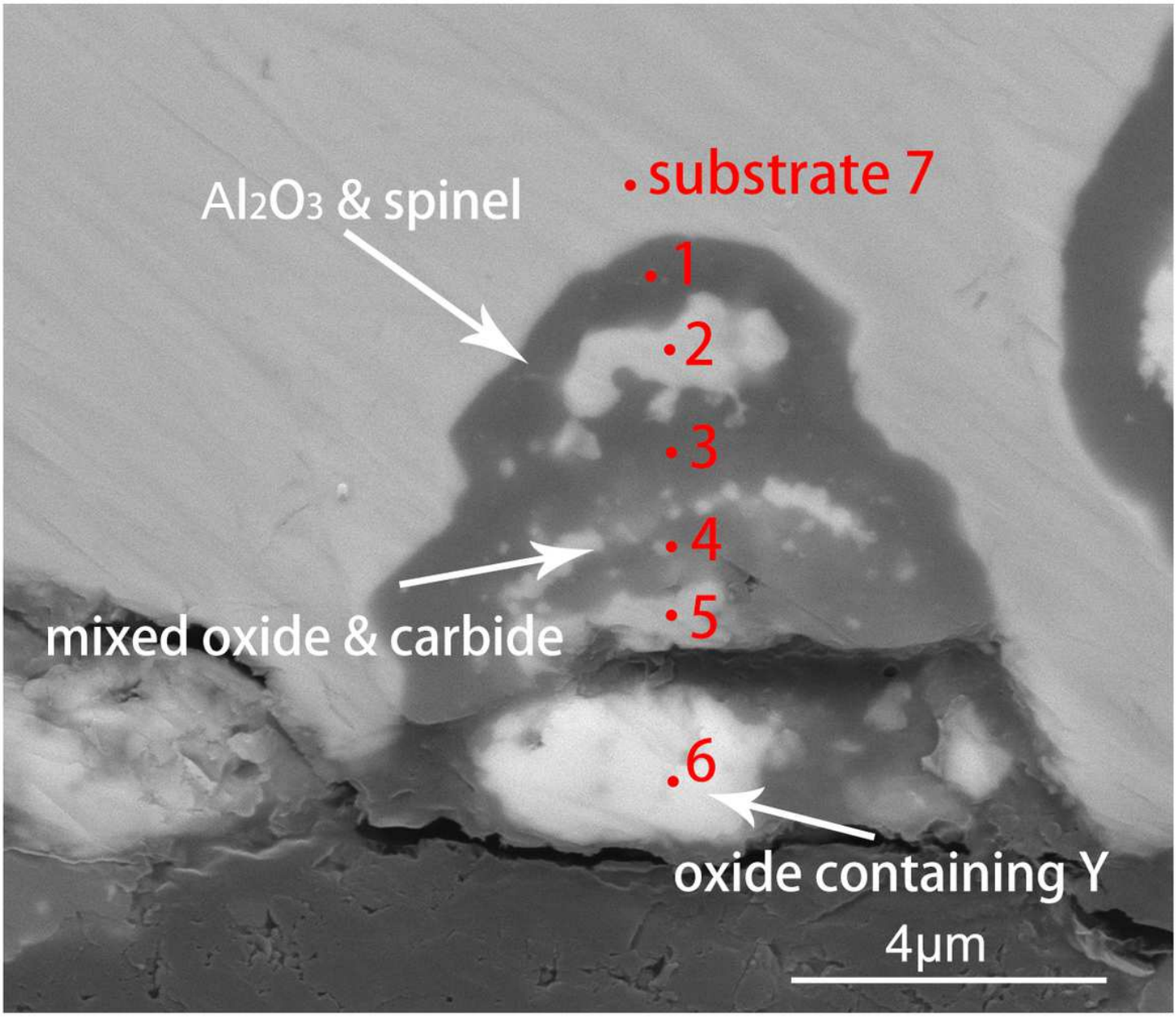

Figure 9

Typical cross-section of surface layer for the Ni-based single crystal superalloy